NASA-TM

Reprinted from

X-Ray and Extreme Ultraviolet Optics

NASA
IN-74-TM
(Oovraript
7718
p. 19

9–11 July 1995
San Diego, California

P
PROCEEDINGS
SERIES

Volume 2515

Advanced X-ray Astrophysics Facility
AXAF — an overview

M. C. Weisskopf, S. L. O'Dell, and R. F. Elsner

Space Sciences Laboratory
Marshall Space Flight Center, Huntsville, Alabama 35812

L. P. Van Speybroeck

Smithsonian Astrophysical Observatory
Center for Astrophysics, Cambridge, Massachusetts 02138

Abstract

The Advanced X-ray Astrophysics Facility (AXAF) is the x-ray component of NASA's Great Observatories. To be launched in late 1998, AXAF will provide unprecedented capabilities for high-resolution imaging, spectrometric imaging, and high-resolution dispersive spectroscopy, over the x-ray band from about 0.1 keV to 10 keV. With these capabilities, AXAF observations will address many of the outstanding questions in astronomy, astrophysics, and cosmology.

Keywords: space missions, x-ray astronomy, x-ray optics, x-ray instrumentation, x-ray spectroscopy

1   INTRODUCTION

In late 1998, the Advanced X-ray Astrophysics Facility (AXAF) will join the Hubble Space Telescope (HST) and the Compton Gamma-Ray Observatory (CGRO) as one of NASA's Great Observatories. As the most sensitive high-resolution x-ray observatory yet planned, AXAF will be a unique scientific facility for use by the general astronomical community. AXAF will provide exceptional capabilities (§5) for x-ray imaging, spectrometric imaging, and dispersive spectroscopy over the energy range 0.1 keV to 10 keV. In very broad terms, the scientific objectives of AXAF are these:

1. To determine the nature of celestial objects and phenomena.

2. To understand the physical processes occurring in cosmic sources.

3. To investigate the history, evolution, and structure of the universe.

NASA Marshall Space Flight Center (MSFC) manages the AXAF Project with scientific and technical support from the Smithsonian Astrophysical Observatory (SAO); TRW Space and Electronics Group is the prime contractor and provides overall systems engineering & integration. The Project Scientist, Martin Weisskopf (MSFC), is responsible for scientific oversight of the AXAF Project; the Telescope Scientist, Leon Van Speybroeck (SAO), has specific responsibility for scientific oversight of the AXAF optics. The Project Scientist also chairs the AXAF Science Working Group — the Telescope Scientist, the 4 Instrument Principal Investigators, 6 Interdisciplinary Scientists, and the director of the AXAF Science Center — which provides additional scientific guidance to the Project.

In this overview (see also Refs. [1], [2], [3], and [4]), we first briefly describe the AXAF flight system (§1.1), calibration plans (§1.2), and operations concept (§1.3). Next, we provide more details on the AXAF flight system — the Telescope System (§2), the Integrated Science Instruments Module (§1.2), and the Spacecraft System (§4). We conclude with a summary of the predicted scientific performance (§5) of AXAF's key science components — namely, the High-Resolution Mirror Assembly (HRMA, §2.1), the Objective Transmission Gratings (OTGs, §2.4), and the focal-plane science instruments (§3.2).

1.1 Flight system

AXAF is NASA's flagship x-ray-astronomy mission, designed to serve the scientific community for at least 5 years. AXAF is the largest existing or planned x-ray-astronomy observatory (see Fig. 1), comparable in length to the Hubble Space Telescope (HST).
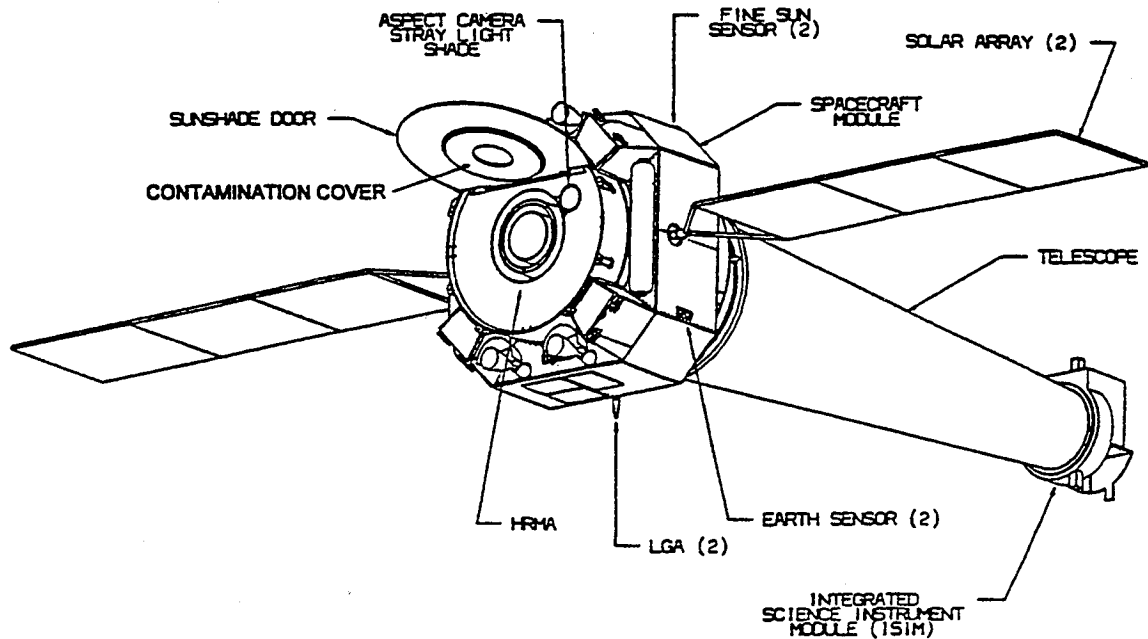

Figure 1: Schematic of the deployed AXAF. The fully deployed AXAF is 13.8-m (45.3-ft) long, with a 19.5-m (64-ft) solar-array wing span and a 4500-kg (5-ton) on-orbit mass.

The AXAF flight system comprises three systems (see Fig. 1 and Fig. 2) — namely, the Telescope System (§2), the Integrated Science Instruments Module (ISIM, §3), and the Spacecraft Module (§4). Eastman Kodak Company (EKC) Commercial & Government Systems is the principal subcontractor for the Telescope System;

Ball Aerospace Systems Division (BASD) is the principal subcontractor for the ISIM; and TRW, the prime contractor, is responsible for the Spacecraft Module.
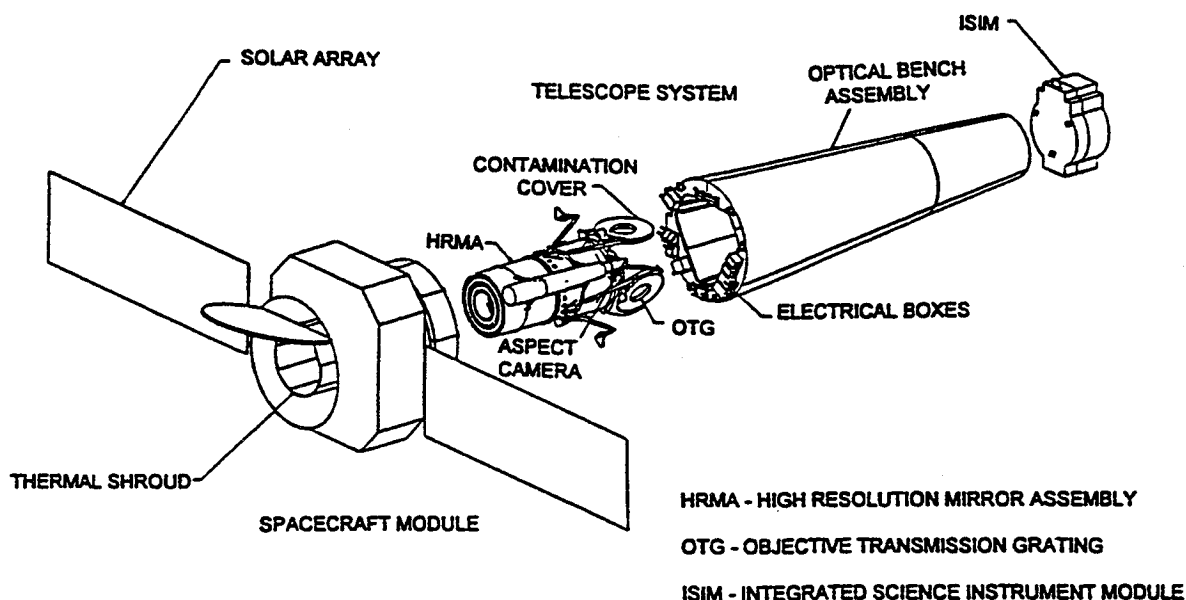

Figure 2: Expanded view of AXAF. The Spacecraft Module, Telescope System, and Integrated Science Instrument Module (ISIM) constitute the AXAF flight system.

Critical to AXAF's scientific success are its precision x-ray optics (§2.1) and its state-of-the-art objective transmission gratings (§2.4) and focal-plane detectors (§3.2). Also important to its success is the unprecedented precision to which AXAF will be calibrated (§1.2).

1.2 Calibration

The AXAF science instruments (gratings and detectors) and x-ray optics will undergo extensive scientific characterization and calibration. There are essentially three calibration phases for the optics and instrumentation — subsystem-level, system-level, and on-orbit. The calibration will require an extensive modeling effort, to be coordinated by the AXAF Science Center (§1.3). Fitting complex models of the optics, gratings, and detectors to the aggregate data in essence constitutes the calibration.

The science-instrument developers will characterize and calibrate their instruments to the extent possible,[5,6] prior to the system-level scientific calibration. Subsystem-level calibrations of each detector will include x-ray efficiency, energy resolution and scale, spatial resolution and scale, and spatial variation. Subsystem-level calibrations of each grating will include transmission efficiency (in several orders) of individual facets and laser optical measurements of line spacing and uniformity. Because the system-level calibration uses only a finite number of discrete energies, SAO is conducting high-energy-resolution reflectance measurements[7,8] of witness flats at the National Synchrotron Light Source (Brookhaven National Laboratory). These data provide a means for interpolating the energy dependence of the effective area of the flight optics, which is particularly critical near the atomic absorption edges of the coating. Additional data required to model the AXAF optics come from metrology of the mirrors and structural models for the mirror assembly.

A calibration team — comprised of personnel from the science-instrument teams, SAO, MSFC, and TRW and its subcontractors — will conduct the science system-level calibration at MSFC's X-Ray Calibration Facility (XRCF). The XRCF, the largest facility of its type, is 520-m (1700-ft) long, to reduce the effects of finite distance between the x-ray sources and the telescope. MSFC is responsible for the XRCF's x-ray source system,[9] comprising stationary- and rotating-anode electron-impact sources, a Penning source,[10] a double-crystal monochromator, and a grating monochromator. SAO is responsible for the x-ray detection system, comprising a microchannel-plate High-Speed Imager (HSI), flow proportional counters, and solid-state detectors. A focal-plane array of these detectors allows calibration of AXAF's x-ray optics and transmission gratings independent of the flight detectors; non-focal-plane flow proportional counters and solid-state detectors allow normalization and mapping of the x-ray beam. Finally, the calibration team will calibrate all flight configurations of the optics, gratings, and focal-plane detectors.

On-orbit calibrations will confirm that the ground calibration has successfully transferred to orbit or indicate necessary adjustments to the calibration models. This confirmation is particularly important because some effects (such as finite-distance and gravitational distortion) cannot be fully compensated during the ground calibration, except through modeling. Furthermore, because grazing-incidence optics are quite sensitive to particulate[11,12] and molecular[13] contamination, AXAF will employ radioactive sources (forward of the optics) to confirm successful transfer of the flux scale.[14] Thereafter, measurements early in the mission will establish celestial calibration sources for future reference during the mission or by other missions.

1.3 Operations

To enhance the observing efficiency of the facility, AXAF's orbit will be highly elliptical. To achieve this orbit, the National Space Transportation System (NSTS) Shuttle will first place the AXAF into a low earth orbit. After deployment from the Orbiter's cargo bay, the Inertial Upper Stage (IUS) — developed by the Boeing Corporation — will place AXAF into a transfer orbit, with a 61,000-km apogee and 280-km perigee. Finally, AXAF's Integral Propulsion Subsystem (IPS, §4.6) will complete the insertion into the operational orbit, with a 140,000-km apogee and 10,000-km perigee. For this orbit, AXAF spends 80% of its time in the low-background environment outside the earth's radiation belts and it experiences only infrequent occultation by the earth; thus the observing efficiency is significantly higher than it would be for a low-earth-orbit mission.

Figure 3 illustrates the AXAF operations concept. The primary elements in AXAF operations are the Deep-Space Network (DSN), the Operations Control Center (OCC), the AXAF Science Center (ASC), and the science community.

NASA's Deep-Space Network (DSN) will provide communications with AXAF. Under nominal operating conditions, command uploads through DSN will occur at 24-h intervals and load 72 h of commands. Telemetry downloads to DSN will occur at 8-h intervals to retrieve data from one of AXAF's two solid-state recorders, each capable of storing over 16 h of data. To accommodate efficiently communications during its highly elliptical orbit, AXAF requires use of DSN's 26-m and 34-m dishes and download rates of 512 kbps and 256 kbps.

The Operations Control Center (OCC) at MSFC provides the DSN with command and control uploads and is responsible for the health, safety, and operation of AXAF. The OCC monitors the telemetry stream for engineering data and forwards the science data (with the engineering data) to the AXAF Science Center (ASC). In addition, the OCC develops the detailed observation time line, based upon observation requests from the ASC.

The AXAF Science Center — operated by the Smithsonian Astrophysical Observatory (SAO) — is the focal point for AXAF science. The ASC is responsible for integrating successful observing proposals into observation requests, reviewing the OCC's detailed time line, receiving and processing the science data, and distributing the data to the scientific community. The ASC is a service to the user community: It will provide user assistance and software tools for proposal preparation, data processing, data archiving and retrieval, and scientific analysis.
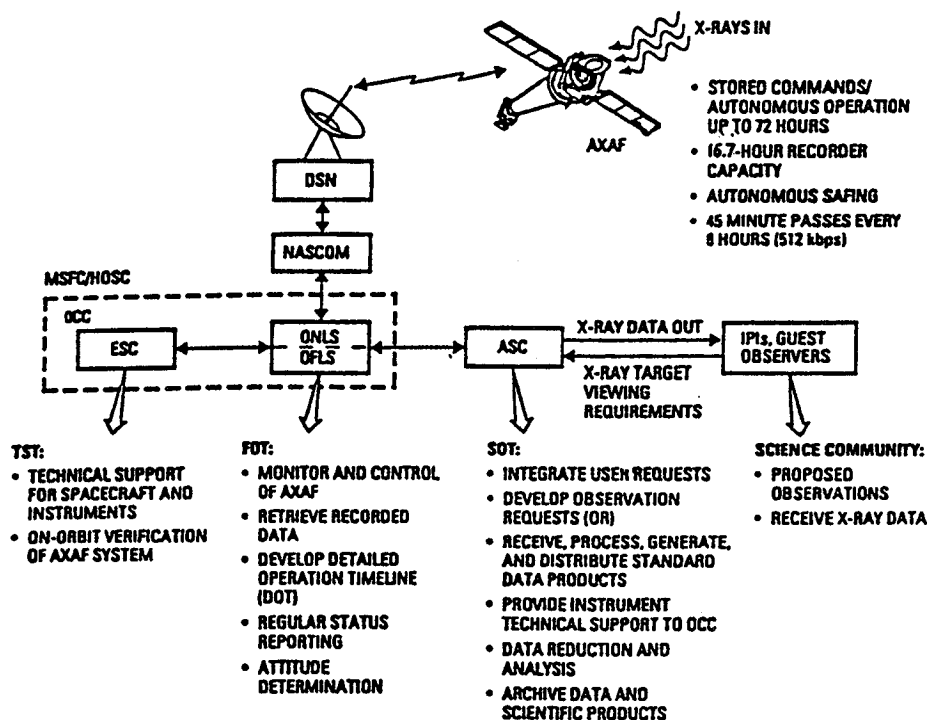
Figure 3: AXAF operations concept, which encompasses the scientific user community, the AXAF Science Center (ASC), the Operations Control Center (OCC), and the Deep-Space Network (DSN).

2 TELESCOPE SYSTEM

The AXAF Telescope System comprises four assemblies: the High-Resolution Mirror Assembly (HRMA, §2.1); the Optical Bench Assembly (OBA, §2.2); the Support Structure Assembly (SSA, §2.3); and the Objective Transmission Gratings (OTGs, §2.4). Of particular importance to AXAF's scientific performance are the HRMA (§2.1) and the OTGs (§2.4).

2.1 High-Resolution Mirror Assembly

The High-Resolution Mirror Assembly (HRMA, see Fig. 2) houses the precision x-ray optics which is the foundation for AXAF's unique capabilities for high-resolution imaging and dispersive spectroscopy. It comprises 4 nested, co-axial, confocal, Wolter-1 (paraboloid–hyperboloid) mirror pairs. With a 10-m (32.8-ft) focal length, the HRMA's plate scale is about 20.5 arcsec/mm, corresponding to about 48.8 micron/arcsec.

Hughes Danbury Optical Systems (HDOS) successfully fabricated the 8 AXAF flight mirrors (4 mirror pairs), completing them and associated metrology ahead of schedule in early 1995. Each mirror element is 84-cm (33-in) long, made of Zerodur glass from Schott Glaswerke, Germany. Table 1 gives the intersection diameter, mean grazing angle, and effective per-surface microroughness (at spatial frequencies between 1 and 1000 mm^{-1} and away from the ends) for each mirror pair. For historical reasons, shell numbering from outside inward is 1, 3, 4, and 6.

The fabricated mirrors are excellent.[15] They are better than specification and at least comparable to goals.

Table 1: Mirror parameters.

Shell number	Diameter [cm]	Diameter [in]	Grazing angle [mrad]	Grazing angle [arcmin]	Roughness [Å]
1	120	47.2	14.9	51	3.2
3	97	38.0	12.0	41	1.9
4	85	33.6	10.6	36	2.1
6	63	25.0	7.9	27	2.5

Indeed, the highly successful smoothing runs produced surface microroughness (Table 1) significantly better than goals. As a consequence, diffractive scattering from surface roughness will be small over the entire AXAF energy range, resulting in an encircled-energy function (integrated fractional included flux of the point response function) which is only weakly dependent on energy (§5.1 and Fig. 7).

Optical Coating Laboratory Inc. (OCLI) is coating the flight mirrors with sputtered iridium. Process-development and qualification coating runs have consistently achieved excellent deposition, with no significant increase in surface roughness. SAO has determined that the reflectance of witness flats is better than specification and corresponds approximately to 95%-bulk-density iridium. Such an iridium coating results in an AXAF high-energy effective area (§5.1 and Fig. 8) which is significantly higher than could be achieved with a gold coating.

After receiving the iridium-coated flight mirrors from OCLI, EKC will align and assemble[16-18] (in a vertical alignment tower) the 8 mirrors (4 mirror pairs) into the HRMA. The basic mounting scheme is to attach each mirror (through bonded flexures) to low-moisture-desorption graphite-composite cylindrical sleeves, which have been bonded at their ends to a central aperture plate, which in turn attaches to an outer cylinder assembly. Alignment accuracy and stability are, of course, essential in order to profit fully from the excellent figure of the fabricated flight mirrors.

Besides the optics subassembly described above, the HRMA includes other subassemblies and components to maintain the quality of the optics. Thermal pre- and post-collimators and heaters maintain the optics subassembly in a stable thermal environment, in order to minimize thermally induced mirror distortions and alignment shifts. Forward and aft contamination covers prevent external particulate and molecular contamination from entering the optics cavity, in order to minimize changes in contamination which could compromise the calibration.[13] In addition, the HRMA includes a fiducial-light transfer system — a periscope to transfer, to the aspect camera (§4.1), light emitted by fiducial lights on the focal-plane science instruments.

2.2 Optical Bench Assembly

The Optical Bench Assembly (OBA) is basically the "tube" of the telescope (see Fig. 2), which must maintain alignment of the HRMA (§2.1) with the focal-plane detectors in the Integrated Science Instrument Module (ISIM, §3). To accomplish this, the OBA is fabricated from a low-moisture-desorption graphite composite and includes thermal-control hardware.

The OBA also provides hardware for attaching the HRMA (§2.1) and the Spacecraft System (§4) at the forward end, and the ISIM (§3) at the aft end. In addition, the OBA serves as a mounting interface for x-ray baffles, for Telescope System electronics, and for power and communications cables between the ISIM and the Spacecraft Module.

2.3 Support Structure Assembly

The Support Structure Assembly (SSA) connects the HRMA (§2.1) to the OBA (§2.2) and serves as the mounting interface for all hardware which must be close to the HRMA. In particular, the SSA provides attachments for thermal-control hardware and for Telescope System mechanisms and associated control electronics — namely, for the drives for the aft contamination cover and for the OTGs (§2.4). In addition, the SSA provides for mounting the aspect camera and the Inertial Reference Unit (IRU), both of which are elements of the Pointing Control and Aspect Determination (PCAD, §4.1) subsystem.

2.4 Objective Transmission Gratings

Both of the Objective Transmission Gratings (OTGs) — the Low-Energy Transmission Grating (LETG, §2.4.1) and the High-Energy Transmission Grating (HETG, §2.4.1) — mount on the SSA (§2.3) aft of the HRMA (§2.1). When AXAF commences orbital operations, the respective mechanism opens (permanently) the aft contamination cover and inserts either the LETG or HETG into the optical path for dispersive spectroscopy. Of course, both the LETG and HETG are retracted for imaging.
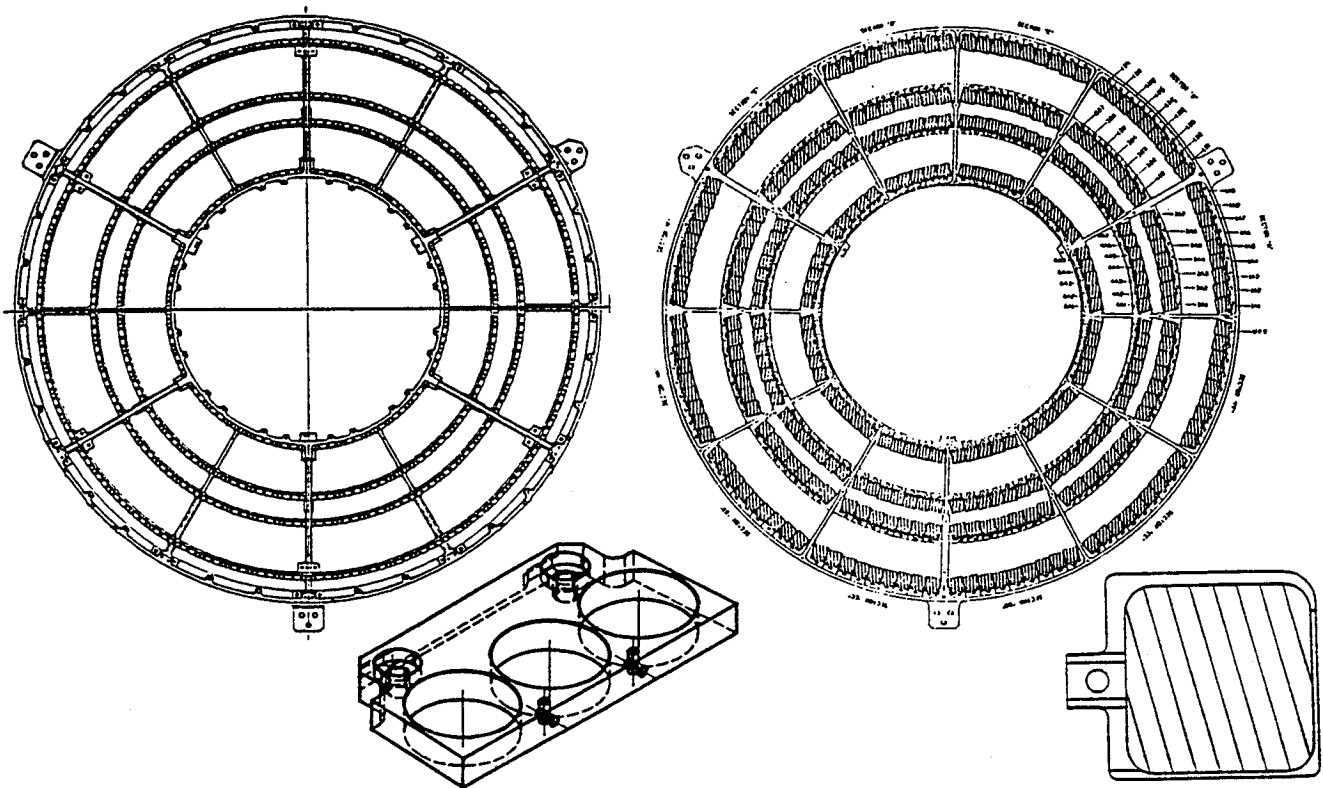
Figure 4: Schematic of AXAF's objective transmission gratings. The left panel shows the LETG's Grating-Element Support Structure (GESS) without grating modules and facets (left inset). The right panel shows the HETG Element Support Structure with grating frames and facets (right inset).

For the LETG and the HETG, hundreds of individual co-aligned grating facets lie on a grating support structure, in 4 annuli which intercept rays exiting the HRMA's 4 mirror shells. In order to optimize the energy resolution, the grating support structure holds the grating facets close to the Rowland toroid which intercepts the focal plane; the focal-plane spectroscopy detectors — HRC-S (§3.2.1) and ACIS-S (§3.2.2) — also approximately conform to the same Rowland circle.

2.4.1 Low-Energy Transmission Grating (LETG)

The Low-Energy Transmission Grating (LETG) will provide high-resolution dispersive spectroscopy at the lower end of the AXAF energy range. Albert Brinkman, of the Space Research Organization of the Netherlands (SRON), is the Instrument Principal Investigator. SRON is developing the LETG in collaboration with the Max Planck Institut für Extraterrestische Physik (MPE).

The LETG (Fig. 4, left panel) has 540 1.6-cm (0.63-in) diameter grating facets, 3 per grating module, mounted on the LETG's aluminum Grating-Element Support Structure (GESS). Ultraviolet contact lithography produces an integrated all-gold facet (grating bars and supporting grids), which is bonded to a stainless-steel facet ring. An individual grating facet has 0.43-micron-thick-gold grating bars, with a 50% filling factor and a 9920-Å period, resulting in a 1.15-Å/mm dispersion at the read-out detector. The primary read-out detector for the LETG is the HRC-S (§3.2.1). Section 5.4 summarizes the expected performance of the LETG spectrometer.

2.4.2 High-Energy Transmission Grating (HETG)

The High-Energy Transmission Grating (HETG) will provide high-resolution dispersive spectroscopy at the higher end of the AXAF energy range. Claude Canizares, of the Massachusetts Institute of Technology (MIT) Center for Space Research (CSR), is the Instrument Principal Investigator. The MIT CSR is developing the grating facets in collaboration with MIT's Nanostructures Laboratory.

The HETG (Fig. 4, right panel) has 336 2.5-cm (1.0-in) square grating facets, each in a grating frame, mounted on the aluminum HETG-Element Support Structure (HESS). Microlithographic fabrication using laser interference patterns produces the grating facet, comprising gold grating bars with 50% filling factor on a polyimide substrate. The HETG uses gratings with 2 different periods which are oriented to produce slightly different dispersion directions, thus forming a shallow "X" image on the read-out detector. To better match the spectral resolution to the energy dependence of the effective area, the Medium-Energy Grating (MEG) occupies HESS annuli corresponding to the outer two HRMA mirror shells (*i.e.*, shells 1 and 3); the High-Energy Grating (HEG), those corresponding to the inner two HRMA mirror shells (*i.e.*, shells 4 and 6). The MEG has 0.40-micron-thick-gold grating bars on 0.50-micron-thick polyimide, with a 4000-Å period, resulting in a 2.85-Å/mm dispersion at the read-out detector; the HEG, 0.70-micron-thick-gold grating bars on 1.0-micron-thick polyimide, with a 2000-Å period, resulting in a 5.70-Å/mm dispersion. The primary read-out detector for the HETG is the ACIS-S (§3.2.2). Section 5.5 summarizes the expected performance of the HETG spectrometer.

3   INTEGRATED SCIENCE INSTRUMENTS MODULE

The Integrated Science Instruments Module (ISIM) comprises the Science Instrument Module (SIM, §3.1) and the two focal-plane science instruments (§3.2) — namely, the High-Resolution Camera (HRC, §3.2.1) and the AXAF CCD Imaging Spectrometer (ACIS, §3.2.2). The ISIM, of course, resides (Fig. 2) at the end of the optical bench (§2.2) opposite the HRMA (§2.1).

3.1   Science Instruments Module

The Science Instruments Module (SIM) houses the focal-plane science instruments (§3.2), providing for them a translating mechanical mount, a controlled thermal environment, venting paths, electrical-power connections to the EPS (§4.3), and command and telemetry interfaces with the CCDM (§4.2).

The SIM positioning assembly translates the focal-plane assembly in two directions: Translation parallel to AXAF's optical axis focuses the telescope; translation perpendicular (in one dimension) places the selected focal-plane detector at the desired aim point. Because focusing the telescope is essential for optimizing the image quality, the SIM's positioning assembly must focus to within 25 micron (0.001 in) and has a focus range of ± 1 cm (± 0.4 in) to ensure best-focus capture throughout the mission. In order to place any of the focal-plane instruments at a desired aim point, the range for transverse positioning is 45 cm (18 in); the required positioning accuracy in this direction is 0.25 mm (0.01 in), corresponding to about 5 arcsec for the HRMA's plate scale (§2.1).

Because focal-plane detectors are sensitive to stray ultraviolet or visible light (from the sun or bright earth), the SIM translation table incorporates an extensive baffling system against stray light in the gap between the stationary and translating parts. Interior to the SIM instrument cavity, the individual focal-plane instruments provide most of the stray-light protection. The combined baffling system ensures that nonpenetrating radiation contributes negligibly to the instrumental backgrounds, which are intrinsically very low.

3.2 Focal-plane science instruments

AXAF has two focal-plane science instruments — the High-Resolution Camera (HRC, §3.2.1) and the AXAF CCD Imaging Spectrometer (ACIS, §3.2.2). Each focal-plane science instrument has two focal-plane detectors, one optimized for imaging and the other optimized for read-out of the spectrum dispersed by the Objective Transmission Gratings (§2.4). Each focal-plane detector operates in photon-counting mode and has a very low internal background.

3.2.1 High-Resolution Camera

The High-Resolution Camera (HRC) provides two microchannel-plate (MCP) detectors — HRC-I for high-resolution imaging and HRC-S for high-resolution dispersive spectroscopy. Steve Murray, of the Smithsonian Astrophysical Observatory (SAO), is the Instrument Principal Investigator.

Besides the two photocathode-coated microchannel-plate detectors and associated fiducial lights, the HRC comprises (Fig. 5) the detector housing and door, anti-coincidence shield with photomultiplier tubes, power supplies, electronics, a purge system, and supporting structure and close-out panels. For efficient focusing of the HRMA (§2.1), the HRC has a moveable shutter above the focal plane. To ensure that the detector response remains calibrated, the HRC has radioactive calibration sources in the detector-housing door; to shield the detectors from non-focused x rays, the HRC adds tantalum shielding; to shield the HRC detectors from ultraviolet light, it employs stray-light baffles (not shown in Fig. 5) and a thin-film UV/ion shield over the microchannel plates. The UV and x-ray shielding significantly reduce the contribution of external sources to the HRC background counting rate. Note that the HRC microchannel plates use low-radioactivity glass to achieve a very low internal background — about 0.04 counts/s/cm^2, equivalent to about 0.08 counts/day/arcsec^2!

The HRC-I detector is a large-format, 100-mm (4-in) square microchannel plate, coated with a CsI photocathode to improve the x-ray response. A conventional cross-grid charge detector reads out the photo-induced charge cloud (after an electron gain of over 10 million), sending the signal through a pre-amplifier to the HRC's central electronics assembly for timing and control of event processing. For each detected event, the HRC determines arrival time with a temporal resolution of 16 microsecond, the position with a spatial resolution of about 18 micron (0.37 arcsec), and the pulse height for an energy resolving power of about unity. The effective field of view of the HRC-I is approximately a 32-arcmin square. The primary use of the HRC-I is for high-resolution wide-field imaging (§5.2 and Fig. 8); it also serves as a back-up read-out device for the LETG (§2.4.1).

The HRC-S detector is a 300-mm-by-20-mm (12-in-by-0.8-in) 3-section microchannel plate, coated with a
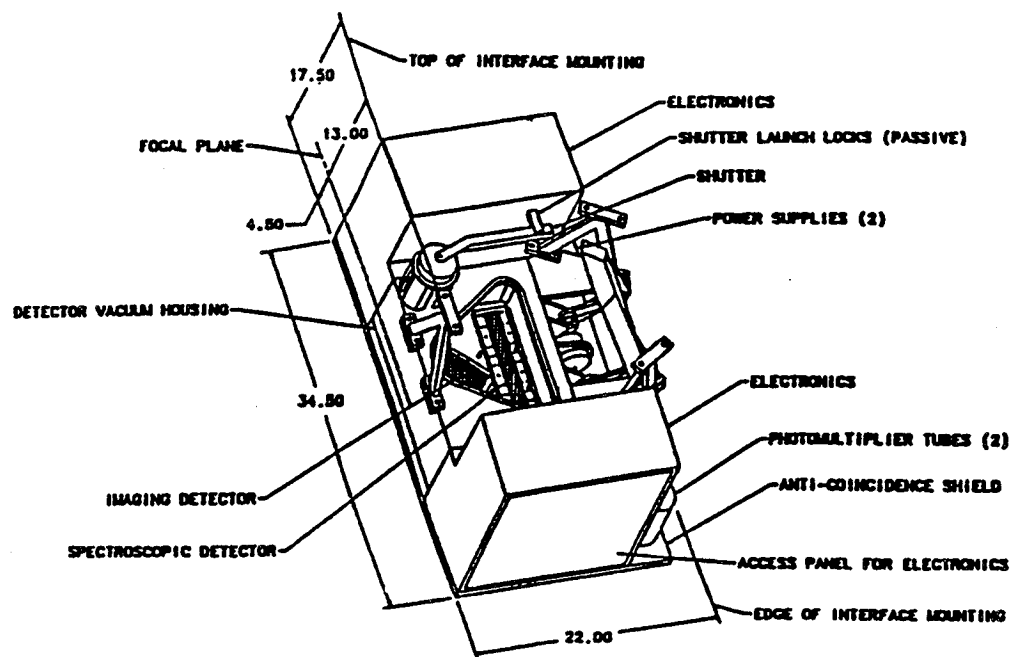
Figure 5: Schematic of the High-Resolution Camera (HRC). The imaging (square) and spectroscopy (strip) microchannel-plate detectors are partly visible through the open detector housing.

KBr photocathode to improve the soft-x-ray response. It uses essentially the same read-out scheme as the HRC-I, except that the read-out grid is a hybrid with wire grid wound in the (narrow) cross-dispersion direction and photo-etched micro-strip grid in the (wide) dispersion direction. The hybrid read-out grid allows tilting the two outside sections slightly toward the gratings in order to conform approximately with the Rowland circle including the transmission grating and the focal plane. The primary use of the HRC-S is for high-resolution spectrometry (§5.4 and Fig. 9) with the LETG (§2.4.1); it also serves as a back-up read-out device for the HETG (§2.4.2).

3.2.2 AXAF CCD Imaging Spectrometer

The AXAF CCD Imaging Spectrometer (ACIS) uses two charge-coupled-device (CCD) detector arrays — ACIS-I for high-resolution spectrometric imaging and ACIS-S for high-resolution dispersive spectroscopy. Gordon Garmire, of the Pennsylvania State University, is the Instrument Principal Investigator. The Massachusetts Institute of Technology (MIT) Center for Space Research (CSR), in collaboration with Lincoln Laboratories, is developing the detector system; Martin Marietta Aerospace is integrating the instrument and providing systems-engineering support.

Besides the two CCD detector arrays and associated fiducial lights, the ACIS comprises (Fig. 6) the detector housing and door, power supplies, digital processor, electronics, a purge system, and supporting structure and close-out panels. To ensure that the ACIS response remains calibrated, it has radioactive calibration sources; to protect the ACIS CCDs from proton-induced displacement damage, it incorporates an aluminum proton shield; to shield the CCDs from visible light, it employs stray-light baffles and a thin-film optical blocking filter over the CCDs. A radiator (not shown in Fig. 6) extends from the SIM on the sun-shaded side to cool passively the detector array to -120 C. This reduces the dark-current noise to a negligible level (much less than 0.1 electrons/pixel/s) compared with the 2-to-3-electron rms noise. Like the HRC, the ACIS has a very low non-x-ray background — about 0.008 counts/s/cm^2, equivalent to less than 0.02 counts/day/arcsec^2!
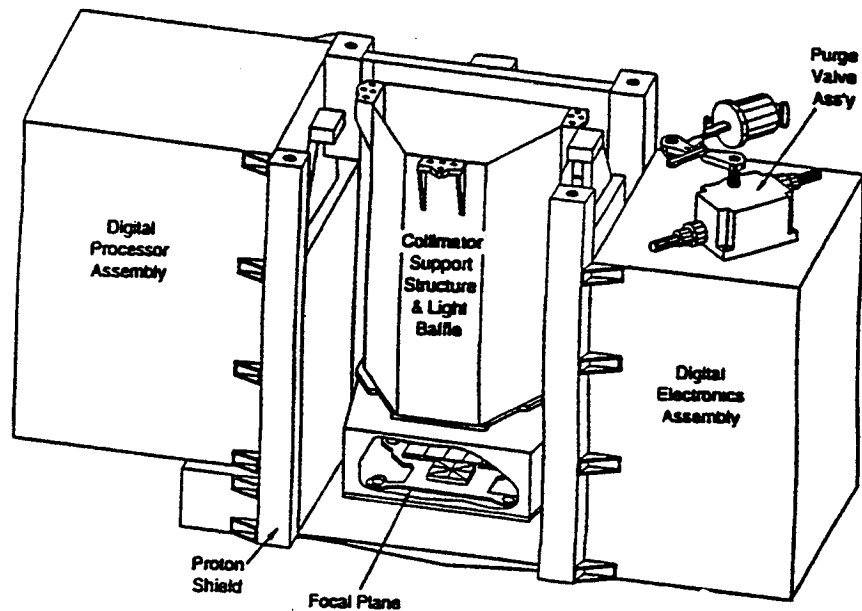
Figure 6: Schematic of the AXAF CCD Imaging Spectrometer (ACIS). The imaging (square) and spectroscopy (strip) CCD arrays are partly visible through the cut-away detector housing.

In addition to the front-illuminated devices already developed, MIT is developing thinned back-illuminated CCDs. The two flavors of CCDs are essentially identical mechanically and electrically; thus any combination of back-illuminated and front-illuminated devices may, in principle, populate the ACIS focal plane. However, there is a science trade between the x-ray performance of the two flavors of ACIS CCDs (Table 2): The front-illuminated devices have better energy resolution; the back-illuminated devices have better low-energy quantum efficiency and (for multiple-pixel events) higher spatial resolution.

Table 2: Preliminary comparison of front-illuminated and back-illuminated ACIS CCDs.

Energy [keV]	Efficiency [%]		Resolution [eV]	
	Front	Back	Front	Back
0.277	< 1	18	···	88
0.525	14	54	55	91
1.49	71	80	80	102
5.90	59	60	134	156

The ACIS focal plane will have some combination of 10 25-mm (1-in) square front-illuminated and back-illuminated CCDs with integral framestores. Each CCD has 1024-by-1024 pixels of 24-micron (0.50 arcsec) size. The ACIS processing can accommodate simultaneously any 6 CCD data streams; it can transfer an entire frame from the imaging area to the framestore in less than 60 ms and read-out the entire framestore in about 2.6 s. A digital electronics assembly digitizes the amplified CCD signal; the processing assembly, which also controls operation of the instrument, then extracts valid x-ray events and processes the data for transmission to the spacecraft's data-management function (§4.2).

ACIS offers 3 CCD-read-out modes: A timed exposure (the standard operating mode) accumulates charge over a commandable 0.1-s-to-10-s period; a continuous read-out extracts and sums a commandable number of CCD rows in about 2.6 ms for high time-resolution measurements, and a diagnostic clocking mode facilitates measurement of the processing-electronics noise. ACIS has 5 data-processing modes: An event mode (the standard operating mode) identifies candidate x-ray events, removes detector artifacts, extracts information for determining location and photon energy, and attaches the time; a timing mode processes data (for the continuous read-out mode), compresses information on position (in one dimension) and amplitude, and time stamps the data; a bright-source imaging mode sacrifices spatial or spectral resolution to preserve as many events as possible under the telemetry-rate constraint; a bright-source spectroscopy mode likewise sacrifices resolution except in the dispersion direction; and a calibration and diagnostic mode provides information on system performance.

The ACIS-I detector is a 2-by-2 array of CCDs; hence, it is approximately a 50-mm (2-in) square. Thus the ACIS-I field of view is approximately a 17-arcmin square. The 4 CCDs tilt slightly toward the HRMA, in order to conform approximately to the optimal focal surface. The primary use of the ACIS-I is for high-resolution medium-field spectrometric imaging (§5.3 and Fig. 8).

The ACIS-S detector is a 1-by-6 array of CCDs; hence, it is approximately a 25-mm-by-150-mm (1-in-by-6-in) rectangle. The 6 CCDs tilt slightly toward the gratings, in order to conform approximately to the Rowland circle including the transmission grating and the focal plane. The primary use of the ACIS-S is for high-resolution spectrometry (§5.5 and Fig. 9) with the HETG (§2.4.2); it also serves as a back-up read-out device for the LETG (§2.4.1). With both OTGs (§2.4) retracted, the central 2 CCDs in the ACIS-S array also provide high-resolution narrow-field spectrometric imaging. This capability is not just a back-up to the ACIS-I: Because the tilt of the ACIS-I array is optimized for medium-field imaging, the ACIS-S actually has somewhat better spatial resolution over a narrow field.

4   SPACECRAFT SYSTEM

The Spacecraft System comprises 7 major subsystems: Pointing Control and Aspect Determination (PCAD, §4.1); Communication, Command, and Data Management (CCDM, §4.2); Electrical Power Subsystem (EPS, §4.3); Thermal Control Subsystem (TCS, §4.4); structures and mechanical subsystem (§4.5); propulsion subsystem (§4.6); and flight software (§4.7). Of particular importance to AXAF's scientific performance is the PCAD subsystem (§4.1).

4.1   Pointing Control and Aspect Determination subsystem

The Pointing Control and Aspect Determination (PCAD) subsystem performs on-board attitude determination, solar-array control, slewing, pointing and dithering control, and momentum management. It thus includes the reaction wheels, Inertial Reference Unit (IRU, or "gyros"), sun sensors, Aspect Camera Assembly, fiducial lights, and all algorithms required to perform its functions. In addition, the PCAD, with the CCDM (§4.2) and flight software (§4.7) subsystems, provides the safing function.

Of special importance to AXAF science is aspect determination, which allows mapping of detector coordinates into celestial coordinates. This mapping must be very stable (rms 0.25-arcsecond radius, relative) for high-definition image reconstruction, and it must be very accurate (rms 1-arcsecond radius, absolute) for source identification. The key assemblies for accurate aspect determination are the Aspect Camera Assembly (an optical telescope and CCD camera, developed by Ball Aerospace Systems Division) and the fiducial-light transfer system (§2.1). Accurate rate-sensing data from the IRU can further refine the post-facto aspect determination and image reconstruction.

4.2 Communication, Command, and Data Management subsystem

The Communication, Command, and Data Management (CCDM) subsystem performs communications (*via* a low-gain antenna) for command uploads and data downloads, command storage and processing, and data acquisition and storage. For other AXAF systems or subsystems, the CCDM subsystem furnishes computational support, timing reference, and switching of primary electrical power. In addition, the CCDM, with the PCAD (§4.1) and flight software (§4.7) subsystems, provides the safing function.

AXAF's internal telemetry rate is 32 kbps: Nominally 24 kbps is science data and 8 kbps is engineering data; but other modes are available for check-out or anomaly handling. Normally, the on-board computer acquires the real-time data, performs rudimentary processing, and stores the data in one of two redundant solid-state recorders for downloads to the DSN (§1.3) through one of the two redundant low-gain antennas.

4.3 Electrical Power Subsystem (EPS)

The Electrical Power Subsystem (EPS) generates, regulates, stores, distributes, conditions, and controls the primary electrical power. Thus it includes the solar array, batteries, electrical interfaces, and distribution and grounding wiring and harnesses. The EPS distributes primary electrical power at about 28 VDC. Besides interfacing with other spacecraft subsystems, the Telescope System, and the Integrated Science Instrument Module (ISIM), the EPS must interface with the ground support equipment, the NSTS Orbiter, and the Inertial Upper Stage (IUS).

4.4 Thermal Control Subsystem (TCS)

The Thermal Control Subsystem (TCS) furnishes passive thermal control (where possible), heaters, and thermostats. In addition, the TCS includes the venting function to accommodate pressure changes during ascent.

Because of sensitivity to thermally induced distortions, effective thermal control is essential for preserving the exceptional imaging capabilities of the HRMA. The Thermal Control System provides a benign environment for the HRMA and thermal isolation for the Telescope System's own thermal-control hardware (§2.1 and §2.2).

4.5 Structures and mechanical subsystem

The structures and mechanical subsystem encompasses the spacecraft structures, mechanical interfaces among spacecraft subsystems and with the telescope system, and structural interfaces with the Inertial Upper Stage (§1.3) and with the NSTS Orbiter. It also includes certain spacecraft appendages, such as the low-gain-antenna booms and the sunshade door assembly.

4.6 Propulsion subsystem

The propulsion subsystem comprises the Integral Propulsion Subsystem (IPS) and the Momentum Unloading Propulsion Subsystem (MUPS). The IPS propels the AXAF into its operational orbit (§1.3) after the Inertial Upper Stage (IUS) has placed the AXAF into a transfer orbit. The MUPS supplies controlled torque for unloading the stored angular momentum of the reaction wheels. (Because of AXAF's high elliptical orbit (§1.3), AXAF does not use magnetic torquers for unloading angular momentum.)

4.7 Flight software

The flight software implements algorithms for attitude determination and control, command and telemetry processing and storage, electrical power monitoring and control, and thermal monitoring and control. In addition, the flight software, with the PCAD (§4.1) and CCDM (§4.2) subsystems, provides the safing function. In the event of a serious spacecraft anomaly, the safing function automatically configures AXAF into one of several pre-defined safe modes, depending upon the nature of the threat. In such safing modes, AXAF can operate autonomously, with little electrical power, for at least 72 h.

5 SCIENTIFIC PERFORMANCE

Critical to AXAF's scientific success are its precision x-ray optics (§2.1) and its state-of-the-art focal-plane detectors (§3.2) and transmission gratings (§2.4). Here we summarize the expected performance of the HRMA (§5.1), the HRC (§5.2) and ACIS (§5.3) imagers, and the LETG (§5.4) and HETG (§5.5) spectrometers. Table 3 compares the the characteristics of AXAF with the principal previous high-resolution x-ray missions[2] — the German Röntgen Satellit (RoSat) and the U.S. Einstein Observatory (HEAO-2). AXAF's very-high-resolution optics, large effective area, and extensive energy range — combined with its low-background high-spatial-resolution detectors and high-spectral-resolution gratings — makes it a powerful tool for point-source detection, high-resolution imaging and spectrometric imaging, and high-resolution spectroscopy of point sources.

Table 3: Comparison of AXAF optics with previous high-resolution x-ray missions.

Property	Unit	AXAF	RoSat	Einstein
Nested mirror shells	number	4	4	4
Mirror-coating material	element (symbol)	iridium (Ir)	gold (Au)	nickel (Ni)
Focal length	m	10.0	2.40	3.45
Plate scale	μm/arcsec	48.8	11.6	16.7
Mirror diameters	cm	63–120	51–83	33–58
Mean grazing angles	arcmin	27–52	83–135	40–70
Angular resolution (FWHM)	arcsec	0.5	3	4
50%-encircled-energy radius @ 1.5 keV	arcsec	0.33	2.5	6.5
Effective area (A_{eff}) @ 1.5 keV	cm^2	780	350	200
Maximum energy for $A_{\text{eff}} > 50$ cm^2	keV	10	2.0	4.0
High-resolution imager	name (type)	HRC (MCP)	HRI (MCP)	HRI (MCP)
High-resolution imaging spectrometer	name (type)	ACIS (CCD)	none	none
Resolving power of gratings	$E/(\Delta E)$	~ 1000	none	~ 100

5.1 HRMA performance

AXAF's x-ray mirrors, as fabricated, are exceptionally good (§2.1 and Ref. [15]). The excellent geometric figure yields a very sharp image core; the very low (less than 3 Å, Table 1) microroughness over most of the surface yields but weak scattering wings, effecting an encircled energy only weakly dependent upon energy. Figure 7

shows the 0.5-arcsec-radius (on-axis) encircled energy as a function of x-ray energy and the (on-axis) encircled energy as a function of radius for various x-ray energies.
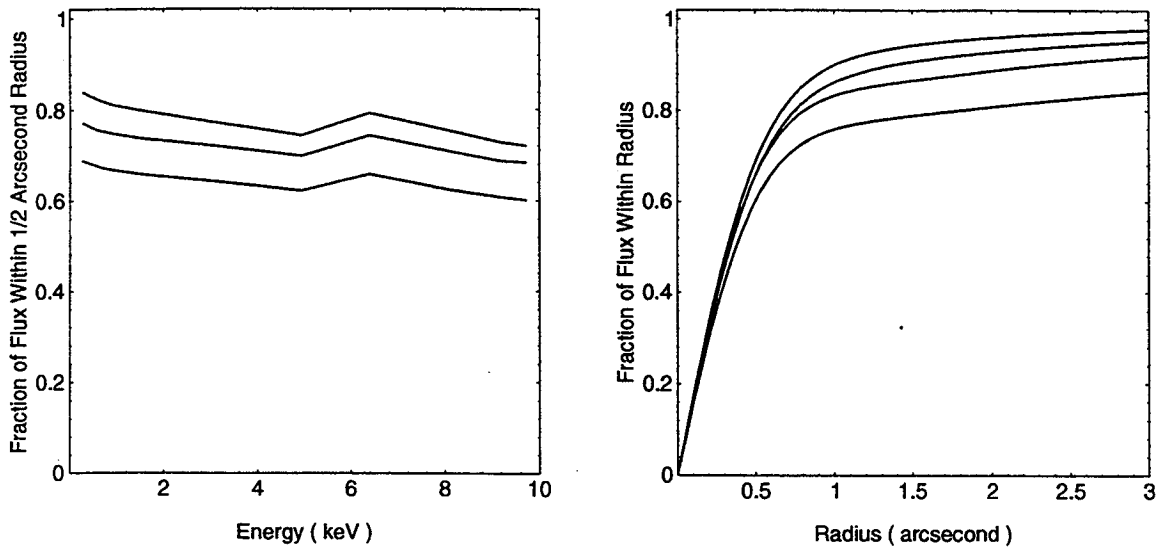

Figure 7: AXAF encircled energy. The left panel shows the predicted 0.5-arcsec-radius encircled energy as a function of energy for the as-built mirrors in a perfectly aligned HRMA (top), in a HRMA aligned at specification (middle), and on-orbit with aspect errors at specification (bottom). The right panel displays the predicted on-orbit encircled energy as a function of radius at (top to bottom) 0.277 keV, 1.49 keV, 6.40 keV, and 9.71 keV.

Figure 8 (left panel) shows the on-axis effective area of the AXAF HRMA. The telescope's design (size and range of grazing angles) and the use of iridium (Ir) as the coating provides a scientifically useful effective area to about 10 keV. (The pronounced depression just above 2.0 keV corresponds to the Ir M_V atomic edge.) For example, in the iron-L spectral region (near 1 keV) the HRMA's effective area is $A_{eff} \approx 780$ cm^2; in the iron-K spectral region (near 6.7 keV) the HRMA's effective area is $A_{eff} \approx 250$ cm^2.
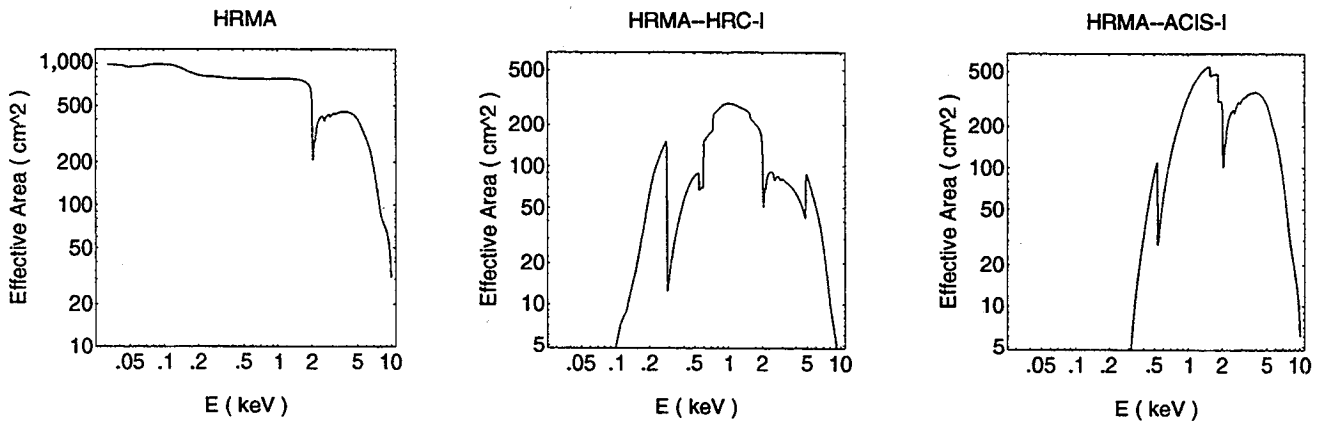

Figure 8: Effective area of the HRMA alone (left), of the HRMA–HRC-I (center), and of the HRMA–ACIS-I (right). The HRC-I efficiency is for a CsI-coated microchannel plate with a UV/ion shield of 700-Å aluminum over 6000-Å Lexan; the ACIS-I efficiency is for a front-illuminated CCD with an optical blocking filter of 1500-Å aluminum over 1000-Å Lexan.

5.2 HRC performance

The HRC focal plane (§3.2.1) contains the HRC-I for wide-field high-resolution imaging (primarily) and the HRC-S for reading the LETG (§2.4.1) spectrometer (primarily). Figure 8 (center panel) shows the predicted (on-axis) net effective area for the HRC-I — i.e., the HRMA effective area, times the HRC-I detection efficiency. In calculating HRC's efficiency, we assume that the photocathode on the HRC-I MCP is CsI, as currently planned.

5.3 ACIS performance

The ACIS focal plane (§3.2.2) contains the ACIS-I for medium-field high-resolution spectrometric imaging (primarily) and the ACIS-S for reading the HETG (§2.4.2) spectrometer (primarily) and for narrow-field high-resolution spectrometric imaging. Figure 8 (right panel) shows the predicted (on-axis) net effective area for the ACIS-I — i.e., the HRMA effective area, times the ACIS-I detection efficiency. In calculating ACIS's efficiency, we assume that the ACIS-I CCDs are front-illuminated; however, that decision is pending.

5.4 LETG spectrometer performance

Figure 9 (left panel) shows the predicted (on-axis) resolving power of the HRMA–LETG for an ideal detector surface — i.e., one conforming to the Rowland circle. Because the HRC-S segmented MCP conforms approximately to the Rowland circle containing either OTG, the expected LETGS — i.e., HRMA–LETG–HRC-S — resolving power is not very different.
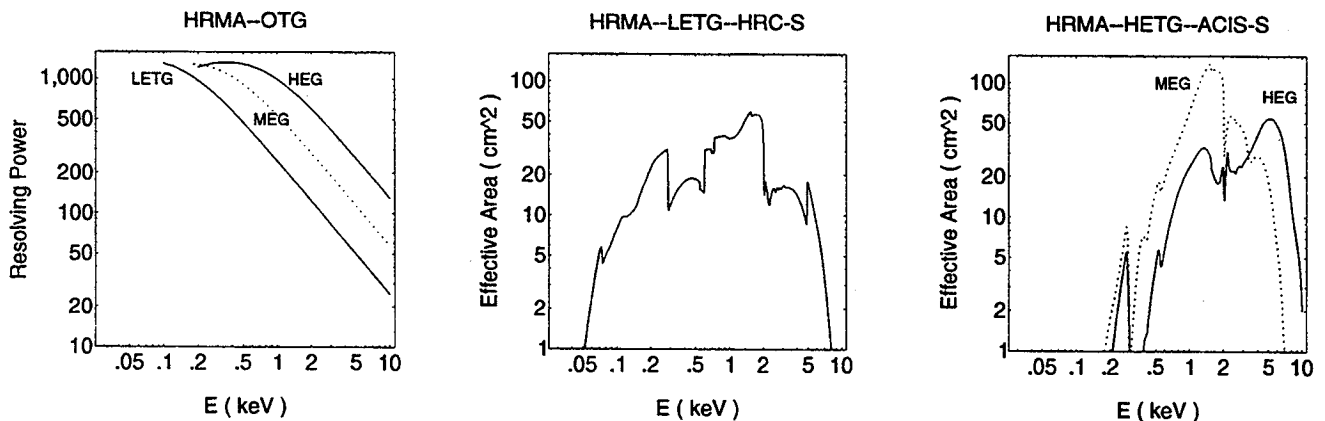

Figure 9: Expected spectroscopic performance of AXAF. The left panel shows the approximate spectral resolving power $E/(\Delta E)$ of the AXAF Objective Transmission Gratings in conjunction with the HRMA. The center panel displays the (summed ± first order) effective area of the LETG spectrometer with the HRC-S as the read-out instrument. The HRC-S efficiency is for a CsI-coated microchannel plate with a UV/ion shield of 300-Å aluminum over 2500-Å Lexan (away from the center of the detector) and 1000-Å aluminum over 2500-Å Lexan (near the center of the detector). The right panel displays the (summed ± first order) effective area of the HETG spectrometer with the ACIS-S as the read-out instrument. The ACIS-S efficiency is for a back-illuminated CCD with a blocking filter of 1500-Å aluminum over 1000-Å Lexan.

The LETG (§2.4.1) spectrometer requires one of the focal-plane detectors as a read-out device. Figure 9 (center panel) shows the predicted (on-axis) net effective area for the LETGS with its primary read-out detector — i.e., the HRMA effective area, times the LETG (summed ± first-order) transmission, times the HRC-S detection

efficiency. In calculating HRC's efficiency, we assume that the HRC-S MCPs are coated with CsI; however, KBr, which gives somewhat different results at the lower energies, may be used as the photocathode.

Below about 0.5 keV, the LETGS achieves high resolving powers (greater than about 500) and has the largest effective area of the AXAF OTGs (*cf.* Fig. 9, center and right panels). Therefore, the LETGS will generally be the preferred instrument for low-energy ($E < 0.5$ keV) high-resolution spectroscopy.

5.5   HETG spectrometer performance

Figure 9 (left panel) shows the predicted (on-axis) resolving power of the HRMA–HETG for an ideal detector surface — *i.e.*, one conforming to the Rowland circle. Because the ACIS-S CCD array conforms approximately to the Rowland circle containing either OTG, the expected HETGS — *i.e.*, HRMA–HETG–ACIS-S — resolving power is not very different. The HETG is actually two gratings, the Medium-Energy Grating (MEG), behind the HRMA's two outer shells, and the High-Energy Grating (HEG), behind the HRMA's two inner shells

The HETG (§2.4.2) spectrometer requires one of the focal-plane detectors as a read-out device. Figure 9 (right panel) shows the predicted (on-axis) net effective area for the HETGS with its primary read-out detector — *i.e.*, the HRMA effective area, times the HETG (summed ± first-order) transmission, times the ACIS-S detection efficiency. In calculating ACIS's efficiency, we assume that the ACIS-S CCDs are back-illuminated; however, that decision is pending.

Below about 2 keV, the HEG achieves high resolving powers (greater than 500); above about 0.5 keV, the effective area of the HETGS-MEG exceeds that of the LETGS (*cf.* Fig. 9, center and right panels). Therefore, the HETGS-MEG will generally be the preferred instrument for medium-energy (0.5 keV $< E < 2$ keV) high-resolution spectroscopy. Finally, the HETGS-HEG will generally be the preferred instrument for high-energy ($E > 2$ keV) high-resolution spectroscopy.

6   ACKNOWLEDGMENTS

7   REFERENCES

[1] *World-Wide Web* homepages, Universal Resource Locators (URLs):
   http://hea-www.harvard.edu/asc/axaf-welcome.html, AXAF Science Center (ASC), SAO.
   http://wwwastro.msfc.nasa.gov/xray/axafps.html, AXAF Project Science, MSFC.
   http://acis.mit.edu/, AXAF CCD Imaging Spectrometer (ACIS), MIT and PSU.
   http://hea-www.harvard.edu/HRC/HomePage.html, High-Resolution Camera (HRC), SAO.

[2] M. V. Zombeck, "Advanced X-ray Astrophysics Facility (AXAF)", in *International School of Space Science Course on "X-ray Astronomy"*, in press. (Harvard/SAO Center for Astrophysics, Preprint Series No. 4003.)

[3] M. C. Weisskopf, "The Advanced X-ray Astrophysics Facility: An overview", *Astrophysical Letters & Communications* **26**, 1–6, 1987.

[4] L. P. Van Speybroeck, "Expected AXAF mirror characteristics and their implications for measurements of the Hubble constant using the Sunyaev–Zel'dovich effect", *Astrophysical Letters & Communications* **26**, 127–146, 1987.

[5] K. A. Flanagan, M. Barbera, S. Murray, and M. Zombeck, "Calibration program for the AXAF High-Resolution Camera", in *EUV, X-Ray, and Gamma-Ray Instrumentation for Astronomy V*, O. H. W. Siegmund and J. V. Vallerga, eds., *Proc. SPIE* **2280**, 243–256, 1994.

[6] C. S. Nelson, T. H. Markert, Y. S. Song, M. L. Schattenburg, D. E. Graessle, K. A. Flanagan, R. L. Blake, J. Bauer, and E. M. Gillikson, "Calibration program for the AXAF High-Resolution Camera", in *EUV, X-Ray, and Gamma-Ray Instrumentation for Astronomy V*, O. H. W. Siegmund and J. V. Vallerga, eds., *Proc. SPIE* **2280**, 191–203, 1994.

[7] D. E. Graessle, T. H. Burbine, J. C. Cobuzzi, E. M. Kellogg, D. A. Schwartz, R. L. Blake, and P. P. Gong, "Reflectance calibrations of AXAF mirror samples at absorption edges using synchrotron radiation", in *Multilayer and Grazing Incidence X-Ray/EUV Optics for Astronomy and Projection Lithography*, R. B. Hoover and A. B. C. Walker Jr., eds., *Proc. SPIE* **1742**, 203–222, 1993.

[8] D. E. Graessle, J. J. Fitch, B. Harris, and R. L. Blake, "Iridium optical constants", in *X-Ray and Extreme Ultraviolet Optics*, R. B. Hoover and A. B. C. Walker Jr., eds., *Proc. SPIE* **2515**, paper 39, these proceedings.

[9] J. J. Kolodziejczak, R. A. Austin, R. F. Elsner, M. K. Joy, M. E. Sulkanen, E. M. Kellogg, and B. J. Wargelin, "X-ray source system at the MSFC X-Ray Calibration Facility," in *X-Ray and Extreme Ultraviolet Optics*, R. B. Hoover and A. B. C. Walker Jr., eds., *Proc. SPIE* **2515**, paper 46, these proceedings.

[10] E. M. Kellogg, B. J. Wargelin, T. J. Norton, R. Eng, and J. J. Kolodziejczak, "Penning source for calibration of x-ray and EUV optics and spectrometers at wavelengths as short as 50 Å," in *X-Ray and Extreme Ultraviolet Optics*, R. B. Hoover and A. B. C. Walker Jr., eds., *Proc. SPIE* **2515**, paper 45, these proceedings.

[11] L. P. Van Speybroeck, "Dust", *Smithsonian Astrophysical Observatory memorandum*, 1987 March 27.

[12] S. L. O'Dell, R. F. Elsner, J. J. Kolodziejczak, M. C. Weisskopf, J. P. Hughes, and L. P. Van Speybroeck, "X-ray evidence for particulate contamination on the AXAF VETA-1 mirrors", in *Multilayer and Grazing Incidence X-Ray/EUV Optics for Astronomy and Projection Lithography*, R. B. Hoover and A. B. C. Walker Jr., eds., *Proc. SPIE* **1742**, 171–182, 1993.

[13] R. F. Elsner, S. L. O'Dell, and M. C. Weisskopf, "Molecular contamination and the calibration of AXAF", in *Multilayer and Grazing Incidence X-Ray/EUV Optics for Astronomy and Projection Lithography*, R. B. Hoover and A. B. C. Walker Jr., eds., *Proc. SPIE* **1742**, 6–12, 1993.

[14] R. F. Elsner, M. K. Joy, S. L. O'Dell, B. D. Ramsey, and M. C. Weisskopf, "Ground-to-orbit transfer of the AXAF-I flux scale," in *Advances in Multilayer and Grazing Incidence X-Ray/EUV/FUV Optics*, R. B. Hoover and A. B. C. Walker Jr., eds., *Proc. SPIE* **2279**, 332–342, 1994.

[15] P. B. Reid, "Fabrication and predicted performance of the Advanced X-ray Astrophysics Facility mirror ensemble," in *X-Ray and Extreme Ultraviolet Optics*, R. B. Hoover and A. B. C. Walker Jr., eds., *Proc. SPIE* **2515**, paper 40, these proceedings.

[16] M. Waldman, "Alignment test system for AXAF's High-Resolution Mirror Assembly," in *X-Ray and Extreme Ultraviolet Optics*, R. B. Hoover and A. B. C. Walker Jr., eds., *Proc. SPIE* **2515**, paper 48, these proceedings.

[17] P. E. Glenn, "Centroid detector for the AXAF alignment test system," in *X-Ray and Extreme Ultraviolet Optics*, R. B. Hoover and A. B. C. Walker Jr., eds., *Proc. SPIE* **2515**, paper 44, these proceedings.

[18] T. S. Lewis, "AXAF alignment test system autocollimating flat error correction," in *X-Ray and Extreme Ultraviolet Optics*, R. B. Hoover and A. B. C. Walker Jr., eds., *Proc. SPIE* **2515**, paper 37, these proceedings.